

A census of new globular clusters in the Galactic bulge

E. Bica¹, S. Ortolani^{2,3,4}, B. Barbuy⁵, and R. A. P. Oliveira⁶

¹ Universidade Federal do Rio Grande do Sul, Departamento de Astronomia, CP 15051, Porto Alegre 91501-970, Brazil

² Università di Padova, Dipartimento di Astronomia, Vicolo dell'Osservatorio 2, I-35122 Padova, Italy

³ INAF-Osservatorio Astronomico di Padova, Vicolo dell'Osservatorio 5, I-35122 Padova, Italy

⁴ Centro di Ateneo di Studi e Attività Spaziali "Giuseppe Colombo" – CISAS, Via Venezia 15, 35131 Padova, Italy

⁵ Universidade de São Paulo, IAG, Rua do Matão 1226, Cidade Universitária, São Paulo 05508-900, Brazil

⁶ Astronomical Observatory, University of Warsaw, Al. Ujazdowskie 4, 00-478 Warszawa, Poland

Received; accepted

ABSTRACT

Context. The number of known globular clusters in the Galactic bulge has been increasing steadily thanks to different new surveys.

Aims. The aim of this study is to provide a census of the newly revealed globular clusters in the Galactic bulge, and analyze their characteristics.

Methods. In recent years, many globular clusters have been discovered or identified. The stellar populations to which they belong are indicated in their original studies: they are mostly bulge clusters, with some identified as disk or halo members. We collected 41 new globular clusters revealed in the last decade and compared them to the known bulge clusters.

Results. The new clusters are intrinsically faint with M_V of around -6.0 mag. The distance to the Sun of the ensemble of well-known and new bulge clusters is compatible with the Galactocentric distance measurements from the Galactic black hole location. The ensemble sample shows metallicity peaks at $[\text{Fe}/\text{H}] \sim -1.08 \pm 0.35$ and -0.51 ± 0.25 dex, confirming previous findings. The age-metallicity relation of the new clusters younger than 10 Gyr is compatible with that of the ex situ samples of the dwarf galaxies Sagittarius, Canis Majoris, and Gaia-Enceladus-Sausage. The clusters with ages between 11.5 and 13.5 Gyr show no age-metallicity relation, because they are all old. This is compatible with their formation in situ in the early Galaxy.

Key words. Galaxy: bulge – globular clusters: general

1. Introduction

The Galactic bulge probably formed due to early mergers within the Λ CDM scenario, and its present configuration was completed later with a buckling bar (e.g. [Queiroz et al. 2020, 2021](#), see also review by [Barbuy et al. 2018a](#)).

The origin of globular clusters (GCs) in the Galactic bulge has become better understood in recent years, thanks to the proper motion measurements from the [Gaia Collaboration et al. \(2023\)](#), and references therein, which allow one to examine their orbits. The nature of the GCs in the Galaxy having two branches in the age-metallicity relation (AMR) was revealed through the derivation of relative ages from ACS/HST data by [Marín-Franch et al. \(2009\)](#). The age-metallicity bifurcation using their data is clearly seen in figure 10 from [Barbuy et al. \(2009\)](#), for example, which shows one branch with the old clusters, in principle formed in situ in the early Galactic bulge, and another branch with the younger ones. This scenario was completed by [Forbes & Bridges \(2010\)](#), making evident that the AMR of the younger clusters fits well that of the dwarf galaxies Sagittarius and Canis Majoris, indicating that they should be accreted ex situ clusters, whereas the older clusters are all old and were formed early on in the history of our Galaxy. According to [Forbes \(2020\)](#), 73 of the known GCs were formed in situ, very early in the Galaxy's history, and 87 were accreted from dwarf galaxies that merged with the Galaxy. Similar classifications were proposed by [Masari et al. \(2019\)](#), [Kruijssen et al. \(2020\)](#), [Pérez-Villegas et al. \(2020, hereafter PV20\)](#), [Callingham et al. \(2022\)](#), [Horta et al.](#)

[\(2023\)](#), and [Belokurov & Kravtsov \(2024\)](#). These authors show the contrast between the age-metallicity plot of in situ clusters, and that of dwarf galaxies.

[Bica et al. \(2016\)](#) identified 43 well-known GCs that would belong to the Galactic bulge, based on an angular distance to the Galactic center lower than 20° , a distance to the Galactic center lower than 3.5 kpc, and a metallicity of $[\text{Fe}/\text{H}] > -1.5$ dex. It is interesting to point out the consideration of metallicity by [Geisler et al. \(2023\)](#), suggesting that clusters with metallicities lower than $[\text{Fe}/\text{H}] \lesssim -1.5$ dex should be identified as more probably being halo clusters. Recently, [Horta et al. \(2023\)](#) and [Belokurov & Kravtsov \(2024\)](#) classified clusters as in situ or ex situ using ages, metallicities, detailed chemistry, total energy, and the z component of the orbital angular momentum.

The sample of Milky Way GCs is still incomplete, as was pointed out, for example, by [Ivanov et al. \(2005\)](#), [Kurtev et al. \(2008\)](#), and [Bica et al. \(2019\)](#), and progress in the detection of newly identified GCs has been made in recent years. Most of the newly revealed clusters were detected in the last five years, due to a combination of the VVV ([Minniti et al. 2010](#)) and VVVX surveys ([Borissova et al. 2018](#)) in J , H , K_S , and proper motions from Gaia Data Release 3 (DR3; [Gaia Collaboration et al. 2023](#)), which allowed decontamination from field stars.

The present work deals with the faint and in general low-mass clusters revealed by several surveys, such as VVV/VVVX in the near-infrared and WISE ([Wright et al. 2010](#)) in the mid-infrared. A number of new confirmed and candidate GCs are now in the process of being identified or having their existences confirmed, and metallicity, reddening, age, distance, and kinemat-

Send offprint requests to: B. Barbuy

ical information is being derived. [Bica et al. \(2019\)](#) present a catalog of Galactic clusters and associations, and compile 200 GCs, plus 94 GC candidates. [Baumgardt & Vasiliev \(2021\)](#) and [Vasiliev & Baumgardt \(2021\)](#) report a list of known GCs, and derived their distances by making use of *Gaia* DR3 ([Gaia Collaboration et al. 2023](#)) proper motions, including some objects in common with the list presented in this paper, as is described below.

In order to study these objects, we compiled the literature data for 39 confirmed clusters and two GC candidates, with 19 of them located in the bulge, considerably increasing the previous number of known bulge clusters ([Bica et al. 2016](#)).

A compilation of newly revealed clusters is described in Sect. 2. Previously identified bulge clusters, with updated data, are reported in Sect. 3. Ages, distances, and metallicities are analyzed in Sect. 4. Conclusions are drawn in Sect. 5.

2. New globular clusters identified in the Galactic bulge

In Table 1 we report 39 newly identified GCs and two GC candidates, basically since the last release of the [Harris \(1996, 2010\)](#) edition¹, hereafter [H10](#) catalog, and in particular since the [Bica et al. \(2016\)](#) review. The table lists coordinates, reddening, distance, metallicity, age, proper motions, absolute magnitudes, and an indication of the stellar populations to which they belong. Most of them can be identified as bulge clusters on the basis of coordinates and distance.

Below, we provide a few comments on some individual clusters. Among the new clusters by [Camargo \(2018\)](#) and [Camargo & Minniti \(2019\)](#), for which proper motions are not explicitly given in the papers, but rather shown in plots, [Camargo 1102](#), [1103](#), and [1104](#) have a different proper motion relative to the field; [Camargo 1107](#), [1108](#), and [1109](#), on the other hand, have an indistinguishable proper motion, but deep VVV color-magnitude diagrams (CMDs), which suggests that they are real clusters. We note, however, that [Gran et al. \(2019\)](#) discard these clusters and dozens of [Minniti](#) clusters based on *Gaia* DR2 and VVV photometry and proper motions, validating only VVV-CL001 ([Minniti et al. 2011](#)) and VVV-CL002 ([Moni Bidin et al. 2011](#)). [Gran et al. \(2019\)](#) state, however, that for these candidates to be real they must have low mass and/or low concentration, or proper motions similar to the field stars (which happens frequently up to 5 mas/yr in their appendix figures). We prefer to move only [Camargo 1105](#) and [1106](#) to the bottom of Table 1 as candidates, and wait for spectroscopy and deeper photometry before definitely confirming or discarding the other [Camargo](#) candidates.

[Horta et al. \(2023\)](#) and [Belokurov & Kravtsov \(2024\)](#) have presented evidence of clusters having formed in situ or having been accreted. Most of the new clusters are not included in the studies, but one case is of particular interest: [FSR 1758](#). [Myeong et al. \(2019\)](#) and [Vasiliev & Baumgardt \(2021\)](#) have shown, based on its retrograde orbit and other properties, that [FSR 1758](#) was accreted from the [Sequoia](#) dwarf galaxy.

[Gran et al. \(2022\)](#) report radial velocities and orbit calculations and conclude that [Gran 1](#) is a bulge GC, formed in situ and that [Gran 2](#), [3](#), and [5](#) might have their origin in the [Gaia-Enceladus-Sausage](#) structure. [Belokurov & Kravtsov \(2024\)](#) instead classify the latter clusters as having formed in situ.

It is also important to point out the measurement of radial velocities with the IGRINS/Gemini spectrograph by [Garro et al. \(2023\)](#), and the calculation of orbits. They find that [Patchick 125](#)

and [Patchick 126](#) are bulge (or halo) clusters, that [Ferrero 54](#), [Gaia 2](#), and [Patchick 122](#) should be disk clusters, and that [VVV-CL160](#) is close to the Galactic center but orbits beyond the solar circle, and therefore has an unclear origin.

Finally, we note that the new clusters that lie outside the range of distances studied here, the ones that have metallicities lower than $[\text{Fe}/\text{H}] \leq -1.5$ dex, and those classified as halo or disk members, are excluded from the plots showing the location of clusters in galactic coordinates, as well as from the metallicity and distance distributions. This amounts to 22 clusters that are not considered; that is, 19 new clusters are included as bulge members.

The reported data were retrieved from the individual papers with the given references. For five of them, distances are also provided, based on *Gaia* data, by [Vasiliev & Baumgardt \(2021\)](#).

Radial velocities are only available for a few clusters, reported in Table 2.

[Minniti et al. \(2021b\)](#) report another 13 cluster candidates that should be further studied: [VVV-CL154](#), and [Minniti 20](#), [39](#), [40](#), [46](#), [47](#), [54](#), [55](#), [56](#), [57](#), [58](#), [59](#), and [60](#), detected in the VVV survey.

3. Previously identified bulge sample

As was mentioned above, [Bica et al. \(2016\)](#) presented a review of GCs that have characteristics of belonging to the Galactic bulge, specified as: a) an angular distance to the Galactic center lower than 20° , b) a distance to the Galactic center shorter than 3.5 kpc, and c) a metallicity of $[\text{Fe}/\text{H}] > -1.5$ dex. Table 3 revises the data available for the 42 GCs identified as belonging to the bulge populations by [Bica et al. \(2016\)](#). In particular, metallicities have been derived for many of them in recent years using high-resolution spectroscopy. We note that for [Terzan 5](#) we adopt the mean of $[\text{Fe}/\text{H}] = -0.3$ dex, corresponding to the dominant population of the various populations, which are estimated to have $[\text{Fe}/\text{H}] = 0.25, -0.3, -0.8$ dex ([Massari et al. 2014](#)); this is compatible with [Origlia & Rich \(2004\)](#). Likewise, for [Liller 1](#) we also adopt a mean of $[\text{Fe}/\text{H}] = -0.3$ dex, which is that of the dominant population and a mean from -0.48 and $+0.27$ dex ([Crociati et al. 2023](#)), and compatible with [Origlia et al. \(2002\)](#). The coordinates of these clusters, not reported in Table 3, can be found in [H10](#); likewise the quantities A_{K_s} , μ_α^* , and μ_δ are given by [Vasiliev & Baumgardt \(2021\)](#).

Distances are reported and given in four different sources, which is useful because there are some discrepant values in the literature. The final distances are adopted from [PV20](#).

The ages were also retrieved from the literature, and are provided in Table 3. Many of the sample objects were observed after the 1990s and different techniques were used to derive their ages. For the sake of homogeneity, we only considered the studies with resolved photometry. Most of the CMDs are from *HST* observations. Exceptions are the deep near-infrared data in K_S versus $J-K_S$ from [Kerber et al. \(2019\)](#) and [Saracino et al. \(2016\)](#) that used the Gemini imager with adaptive optics, and the observations of [UKS 1](#) with the VVV survey; the latter is not deep, reaching just above the turnoff. The isochrone fitting procedures in [Kerber et al. \(2019\)](#), [Ortolani et al. \(2019a\)](#), [Oliveira et al. \(2020\)](#), [Fernández-Trincado et al. \(2020\)](#), and [Souza et al. \(2021, 2023\)](#) employed a statistical Bayesian method with the SIRIUS code ([Souza et al. 2020](#)), based on grids of Dartmouth ([Dotter et al. 2008](#)) and/or BaSTI isochrones ([Pietrinfermi et al. 2006](#)), and a similar procedure was applied by [Kerber et al. \(2018\)](#). [Cohen et al. \(2021\)](#) used the fiducial lines of both the studied clusters and well-known clusters with reliable age determinations

¹ <https://physics.mcmaster.ca/~harris/mwgc.dat>

Table 1. Literature data on the 41 newly identified GCs and candidates, reporting coordinates, reddening, distance to the Sun, metallicity, age, proper motions, magnitudes, and assignment to a Galactic stellar population.

Name	RA (°)	Dec. (°)	ℓ (°)	b (°)	A_{K_s}	d_{\odot} (kpc)	[Fe/H] (dex)	age (Gyr)	μ_{α}^* (mas/yr)	μ_{δ}	M_K	M_V Pop. (mag)	Ref.
Gaia 2	28.138	53.043	132.155	-8.730	0.10	4.9±0.5	-0.90 ± 0.2	10.0±1	-1.31 ± 0.18	1.21 ± 0.19	-5.4 ± 2.0	-3.9	D 1
Ferrero 54	128.451	-44.447	262.803	-2.570	0.60	7.1±0.4	-0.2 ± 0.2	>10	-1.33 ± 0.27	1.31 ± 0.34	-5.87 ± 1.7	-4.1	D 1
Patchick 122	145.628	-52.428	276.340	0.405	0.63	5.6±0.4	-0.5 ± 0.2	>6	-3.72 ± 0.12	3.81 ± 0.12	-6.12 ± 1.0	-4.2	D 1
Garro 1	212.250	-65.620	310.828	-3.944	0.15	15.5±1.0	-0.7 ± 0.2	11.0±1	-4.68 ± 0.47	-1.34 ± 0.45	-7.76 ± 0.5	-5.26	D 2
RLGC 1	244.285	-44.594	336.870	4.303	-	28.8±4.3	-2.2 ± 0.2	12.6	1.04±0.05	0.83 ± 0.04	-	-	H 3
Patchick 125, Gran 3 ^f	256.253	-35.495	349.756	3.424	0.33	10.9±0.5	-1.63 ± 0.14	14	-3.85 ± 0.50	0.64 ± 0.39	-6.1 ± 0.8	-3.8 B/H	1,4
Patchick 126 ^f	256.411	-47.342	340.380	-3.825	0.44	8.6±0.4	-0.7 ± 0.3	>8	-4.75 ± 0.46	-6.68 ± 0.62	-5.56 ± 0.8	-3.5 B/H	1
Gran 2 ^f	257.890	-24.849	359.229	8.587	-	16.6	-1.46 ± 0.1	-	0.19	-2.57	-	-5.92	H 4
Camargo 1102	260.437	-26.544	359.145	5.734	-	8.2±1.2	-1.7 ± 0.2	13.3±1	-	-	-6.3 ± 0.6	B 5	
FSR1758 ^A	262.800	-39.808	349.217	-3.292	-	11.5±1.0	-1.5 ± 0.3	-	-2.19	2.55	-	-	B 6
Minni 48	263.325	-28.001	359.351	2.790	0.45	8.4±1.0	-0.2 ± 0.3	10±2	-3.1 ± 0.4	-6.0 ± 0.5	-9.04 ± 0.66	-6.5	B 7
FSR019	263.910	-21.070	5.499	6.071	0.19	7.2±0.7	-0.5	11	-2.50 ± 0.76	-5.02 ± 0.47	-7.72	-4.62	B 8
FSR1767	263.929	-36.358	352.601	-2.166	0.28	10.6±0.5	-0.7 ± 0.2	11±2	-3.02 ± 0.50	-4.85 ± 0.50	-8.4 ± 1.5	-6.3	B 9
Camargo 1107	264.243	-30.147	357.977	0.956	-	4.0±0.7	-2.2 ± 0.4	13.5±2	-	-	-6.6 ± 0.5	B 10	
ESO393-12	264.657	-35.651	353.514	-2.284	0.23	8.2±0.4	-0.6 ± 0.2	10±2	-2.86 ± 0.47	-5.39 ± 0.44	-7.7 ± 1.5	-5.3	B 9
VVV-CL003	264.728	-29.907	358.405	0.730	0.92	13.2±0.8	-0.1	-	-1.93 ± 0.05	8.33 ± 0.05	-9.92	-6.82	H11,12
VVV-CL002	265.276	-28.845	359.559	0.889	1.07	8.6±0.6	-0.4	>6.5	-9.33 ± 0.07	2.78 ± 0.07	-7.71	-4.61	B11,12
VVV-CL131	265.321	-34.567	354.721	-2.170	0.23	9.0±0.5	-0.6 ± 0.2	10±3	-3.24 ± 0.81	-5.65 ± 0.07	-8.2 ± 1.5	-5.9	B 9
FSR025	265.430	-19.571	7.534	5.649	0.27	7.0±0.6	-0.5	11	-2.61 ± 1.27	-5.23 ± 0.74	-7.31	-4.21	B 8
VVV-CL143	266.150	-33.738	355.788	-2.319	0.21	8.9±0.5	-0.6 ± 0.2	10±3	-3.18 ± 0.91	-6.17 ± 0.85	-8.2 ± 1.3	-5.9	B 9
Camargo 1108	266.518	-30.865	358.404	-1.087	-	3.3±0.5	-1.8 ± 0.3	13.5±1.5	-	-	-8.4 ± 0.5 B/H	-	10
Camargo 1109	266.861	-26.648	2.165	0.844	-	4.3±0.6	-1.5 ± 0.2	12.0±1.5	-	-	-6.4 ± 0.7	B 10	
Minni 22	267.214	-23.061	356.828	-2.729	0.47	7.4±0.3	-1.3 ± 0.3	11.2	-	-	-6.2	B 13	
Gran 5 ^f	267.228	-24.170	4.459	1.838	0.43	4.47	-1.02 ± 0.11	-	-5.32	-9.20	-	-5.95	B 4
ESO456-09	268.476	-32.466	357.882	-3.339	0.18	7.6±0.4	-0.6 ± 0.2	10±2	-3.41 ± 0.71	-4.36 ± 0.75	-8.3 ± 1.5	-6.0	B 9
FSR1776	268.558	-36.152	354.720	-5.249	-	7.2±0.5	0.02 ± 0.14	10±1	-1.9 ± 0.9	-2.6 ± 0.8	-	-	B 14
VVV-CL001	268.677	-24.015	5.268	0.780	-	8.2 ^{+1.84} _{-1.93}	-2.45 ± 0.24	11.9 ^{+3.12} _{-4.05}	-3.41 ± 0.50	-1.97 ± 0.50	-	-	H115,16
FSR1775	269.022	-36.566	354.546	-5.779	0.16	8.9±0.2	-1.1 ± 0.2	10±2	-3.00 ± 0.80	-5.53 ± 0.73	-8.0 ± 1.7	-5.6	B 9
ESO456-29, Gran 1 ^f	269.651	-32.020	358.767	-3.977	0.24	7.9	-1.13 ± 0.06	-	-8.10	-8.01	-	-5.46	B 4
Camargo 1104	271.309	-24.979	5.621	-1.778	-	5.4±1.0	-1.8 ± 0.3	13.5±0.5	-	-	-5.7 ± 1.7	B 5	
Garro 2	271.463	-17.701	12.042	1.656	0.79	5.6±0.8	-1.30 ± 0.2	12±2	-6.07 ± 0.62	-6.15 ± 0.75	-7.52 ± 1.23	-5.44	H 17
Camargo 1103	271.631	-25.162	5.604	-2.121	-	5.0±0.8	-1.8 ± 0.3	13.5±1	-	-	-6.9 ± 1.0	B 5	
VVV-CL160	271.738	-20.011	10.151	0.302	1.71	4.0±0.5	-1.4 ± 0.2	13±2	-2.90 ± 1.28	-16.47 ± 1.31	-7.9 ± 1.5	-5.5	B 18,9
Kronberger 49	272.600	-23.340	7.627	-2.012	0.30	8.3±0.5	-0.2 ± 0.2	11±2	-2.84 ± 0.69	-5.52 ± 0.71	-8.5 ± 1.5	-6.7	B 19,9
Patchick 99	273.946	-29.813	2.488	-6.145	0.09	6.4±0.2	-0.2 ± 0.2	10±2	-2.59 ± 1.51	-5.49 ± 2.02	-7.0 ± 0.6	-5.2	B 20
FSR0009	277.128	-31.907	1.855	-9.529	0.11	6.9±0.2	-1.2 ± 0.3	11±2	-1.39 ± 1.10	-5.22 ± 0.99	-5.8 ± 0.7	-3.4	B 9
Gran 4	278.113	-23.101	10.198	-6.388	0.14	22.5	-1.72 ± 0.32	-	0.46	-3.49	-	-6.45	H 4
RLGC 2	281.368	-5.193	27.631	-1.042	-	15.8±2.4	-2.1 ± 0.3	12.6	-2.41 ± 0.05	-1.85 ± 0.05	-	-	B 3
Riddle 15	287.787	14.833	48.355	2.455	0.52	18.1±0.5	-1.4 ± 0.2	>10	-1.03 ± 0.32	-1.64 ± 0.27	-7.6 ± 0.8	-6.2	H 1
Globular cluster candidates													
Camargo 1106	263.143	-30.280	357.351	1.683	-	4.5±0.4	-1.5 ± 0.3	12.5±1	-	-	-5.7 ± 1.6	B 5	
Camargo 1105	264.141	-28.311	359.479	2.017	-	5.8±0.9	-1.5 ± 0.2	13.0±1	-	-	-6.3 ± 1.0	B 5	

References: 1 Garro et al. (2022a); 2 Garro et al. (2020); 3 Ryu & Lee (2018); 4 Gran et al. (2022) and Gran et al. (2024); 5 Camargo (2018); 6 Barbá et al. (2019); 7 Minniti et al. (2021c); 8 Obasi et al. (2021); 9 Garro et al. (2022b); 10 Camargo & Minniti (2019); 11 Moni Bidin et al. (2011); 12 Minniti et al. (2021b); 13 Minniti et al. (2018); 14 Dias et al. (2022); 15 Minniti et al. (2011), 16 Fernández-Trincado et al. (2021b); 17 Garro et al. (2022c); 18 Minniti et al. (2021a), 19 Ortolani et al. (2012); 20 Garro et al. (2021). ^f or ^A identified as in situ or accreted by Belokurov & Kravtsov (2024). Population: B:bulge, D:Disk, H:Halo, HI:Halo intruder. Errors are adopted from the original papers, when available.

Table 2. Radial velocities available for the new clusters.

Cluster	RV (km.s ⁻¹)	Reference
VVV-CL001	-324.9 ± 0.08	1
FSR1758	226.8 ± 0.08	2
VVV-CL002	-27.3 ± 0.10	3
Patchick 99	92 ± 10	4
Gran 1	76.98 ± 3.62	5
Gran 2	61.24 ± 2.70	5
Gran 3	91.57 ± 5.97	5
Gran 4	-265.28 ± 3.92	5
Gran 5	-59.19 ± 4.93	5

References: 1 Fernández-Trincado et al. (2021b); 2 Villanova et al. (2019); 3 Minniti et al. (2024); 4 Butler et al. (2024); 5 Gran et al. (2024).

to derive their relative ages. Bruzual et al. (1997) employed the early Padova isochrones (Bressan et al. 1993), whereas Renzini

et al. (2018) employed the Victoria-Regina code and isochrones (VandenBerg et al. 2014). Saracino et al. (2016), Ferraro et al. (2021), and Palla et al. (2021) employed fiducial lines and χ^2 minimization to fit isochrones, employing the models mentioned above.

Age determinations using other methods, such as the magnitude difference between the horizontal branch and the main sequence turnoff, integrated spectra models, and M_V calibrations of RR Lyrae stars, were not considered. The ages range from 11.5 to 13.5 Gyr, with an average age of 12.5 Gyr, in agreement with a mean of 12.3 Gyr from Oliveira et al. (2020). Fifteen clusters with no age determination are mostly low-mass and very reddened.

In Table 3 we identify the clusters classified as bulge members according to their orbits by Pérez-Villegas et al. (2020), identified by a ^B. We also indicate, in Tables 1 and 3, the classification of having been formed in situ or accreted, based on the total energy, E , and z component of the orbital angular momentum and further calibrated using the [Al/Fe] abundance ratio, by Belokurov & Kravtsov (2024), indicated by ^I or ^A, corresponding to “in situ” or “accreted.”

Table 3. Bulge GCs from [Bica et al. \(2016\)](#), with distances, ages, and metallicity values from the literature, in order of right ascension. UKS 1 has been added (see text).

Cluster	ℓ ($^{\circ}$)	b ($^{\circ}$)	Adopted (PV20)	Distance to the Sun (kpc)			M_V Ref.(mag.)	[Fe/H] (dex)	Ref.	Age (Gyr)	Ref.
				H10	BV21	Our group					
Terzan 3 ^I	345.08	9.19	8.20 ± 0.82	8.20	7.644 ^{+0.318} _{-0.304}	6.50±1.0	1 -4.82	-1.01±0.08	1, 2	–	–
ESO452-SC11 ^{B,I}	351.91	12.10	6.50 ± 0.65	8.30	7.389 ^{+0.174} _{-0.196}	–	– -4.02	-0.81±0.13	3	–	–
NGC 6256 ^{B,I}	347.79	3.31	6.40 ± 0.64	10.30	7.252 ^{+0.299} _{-0.281}	6.4±1.0	2 -7.15	-1.05±0.13	1	12.9 ± 1.0	1
NGC 6266 ^{B,I}	353.58	7.32	6.41 ± 0.12	6.80	6.412 ^{+0.105} _{-0.104}	6.6±0.5	3 -9.18	-1.18±0.07	4	11.6 ± 0.6	2
NGC 6304 ^{B,I}	355.83	5.38	6.28 ± 0.11	5.9	6.152 ^{+0.130} _{-0.146}	6.07±0.009	4 -7.30	-0.37±0.07	4	12.3 ± 0.8	3
NGC 6316 ^I	357.18	5.76	11.60 ± 1.16	10.40	11.152 ^{+0.393} _{-0.350}	–	– -8.34	-0.50±0.06	1	–	–
NGC 6325 ^I	0.97	8.00	7.80 ± 0.78	7.80	7.533 ^{+0.302} _{-0.314}	6.9±1.0	5 -6.96	-1.38±0.10	1, 2	12.5 ± 0.9	1
NGC 6342 ^{B,I}	4.90	9.73	8.43 ± 0.84	8.50	8.013 ^{+0.235} _{-0.224}	–	– -6.42	-0.55±0.05	5	11.5 ± 1.3	1
NGC 6355 ^I	359.58	5.43	8.70 ± 0.87	9.20	8.655 ^{+0.224} _{-0.230}	8.54±0.19	6 -8.07	-1.39±0.08	6	13.2 ± 1.0	1,4
Terzan 2 ^I	356.32	2.30	7.50 ± 0.75	7.50	7.753 ^{+0.330} _{-0.318}	7.7±0.6	7 -5.88	-0.85±0.04	7	–	–
Terzan 4 ^I	356.02	1.31	6.70 ± 0.67	7.20	7.591 ^{+0.318} _{-0.324}	8.0±0.7	8 -5.74	-1.40±0.05	7, 8	–	–
HP 1 ^{B,I}	357.42	2.12	6.59 ± 0.16	8.20	6.995 ^{+0.144} _{-0.141}	6.59 ^{+0.15} _{-0.15}	9 -6.46	-1.06,-1.20±0.10	9, 7	12.8 ± 0.9	5
Liller 1 ^{B,I}	354.84	-0.16	8.20 ± 0.82	8.20	8.061 ^{+0.353} _{-0.338}	6.5±1.0	8 -7.32	-0.3±0.22	10**	12.0 ± 1.5	6
Terzan 1 ^I	357.57	1.00	6.70 ± 0.67	6.70	5.673 ^{+0.175} _{-0.170}	5.2±0.5	10 -4.41	-1.06±0.13	1	–	–
Ton 2 ^I	350.80	-3.42	6.40 ± 0.64	8.20	6.987 ^{+0.420} _{-0.326}	6.4±1.0	11 -6.17	-0.73±0.13	1	–	–
NGC 6401 ^{B,I}	3.45	3.98	7.70 ± 0.77	10.6	8.064 ^{+0.238} _{-0.241}	12.0±1.0	12 -7.90	-1.12±0.07	1	13.2 ± 1.2	1
Palomar 6 ^I	2.09	1.78	5.80 ± 0.58	5.80	7.047 ^{+0.463} _{-0.433}	7.67±0.19	13 -6.79	-1.10±0.09	11	12.4 ± 0.9	7
Djorg 1 ^I	356.67	-2.48	9.30 ± 0.50	13.70	9.879 ^{+0.628} _{-0.628}	9.3±0.5	14 -6.98	-1.54±0.13	1	–	–
Terzan 5 ^I	3.81	1.67	5.50 ± 0.51	6.90	6.617 ^{+0.150} _{-0.148}	4.6±0.9	8 -7.42	-0.3±0.12	8,12**	12.0 ± 1.0	8
NGC 6440 ^{B,I}	7.73	3.80	8.24 ± 0.82	8.5	8.248 ^{+0.248} _{-0.241}	8.47±0.4	15 -8.75	-0.24±0.05	1, 2	13.0 ± 1.5	9
Terzan 6 ^I	358.57	-2.16	6.80 ± 0.68	6.80	7.271 ^{+0.360} _{-0.343}	7.0±1.0	16 -7.59	-0.43 ± 0.08	13	–	–
UKS 1 ^I	5.13	-0.76	11.1 ± 1.8	7.8	15.581 ^{+0.570} _{-0.530}	10.6±1.5	8 -6.91	-0.98±0.11	14	13.0 ± 1.2	10
Terzan 9 ^I	3.60	-1.99	7.10 ± 0.71	7.10	5.770 ^{+0.333} _{-0.333}	4.9±1.0	17 -3.71	-1.10,-1.40±0.15	15, 7	–	–
ESO456-SC38 ^{B,I}	2.76	-2.50	8.75 ± 0.20	6.30	8.764 ^{+0.178} _{-0.178}	8.75±0.12	18 -7.00	-1.07±0.09	7	12.7 ± 0.7	11
Terzan 10 ^I	4.42	-1.86	10.3 ± 1.0	5.8	10.212 ^{+0.412} _{-0.396}	10.3±1.0	14 -6.35	-1.47±0.02	13	–	–
NGC 6522 ^{B,I}	1.02	-3.93	7.40 ± 0.19	7.70	7.295 ^{+0.241} _{-0.205}	7.62±0.17	19 -7.65	-1.05±0.11	16	12.8 ± 1.0	12
NGC 6528 ^{B,I}	1.14	-4.17	7.70 ± 0.77	7.90	7.829 ^{+0.239} _{-0.239}	7.7±1.0	8 -6.57	-0.17±0.07	17, 9	12.7 ± 1.0	13
NGC 6539 ^I	20.80	6.78	7.85 ± 0.66	7.8	8.165 ^{+0.395} _{-0.379}	–	– -8.29	-0.55±0.06	1	–	–
NGC 6540 ^{B,I}	3.29	-3.31	5.20 ± 0.52	5.30	5.909 ^{+0.278} _{-0.285}	3.50±0.4	20 -6.35	-1.06±0.06	7	–	–
NGC 6553 ^{B,I}	5.25	-3.02	6.75 ± 0.22	6.0	5.332 ^{+0.128} _{-0.123}	5.2±1.0	21 -7.77	-0.27±0.09	18	12.0 ± 2.0	14
NGC 6558 ^{B,I}	0.20	-6.03	8.26 ± 0.53	7.40	7.474 ^{+0.282} _{-0.282}	6.3±1.0	22 -6.44	-1.16±0.08	19	12.3 ± 1.1	1
BH 261 ^{B,I}	3.36	-5.27	6.50 ± 0.65	6.50	6.115 ^{+0.265} _{-0.253}	–	– -4.06	-1.09±0.05	13	–	–
Glimpse02	14.13	-0.64	–	5.50	–	–	– -1.08±0.13	20	–	–	–
Mercer 5	17.59	-0.86	5.50 ± 0.55	–	5.466 ^{+0.523} _{-0.476}	–	– -0.86±0.12	20	–	–	–
NGC 6624 ^{B,I}	2.79	-7.91	8.43 ± 0.11	7.9	8.019 ^{+0.108} _{-0.099}	8.19±0.15	4 -7.49	-0.36±0.12	21	11.7 – 12.0 ± 0.63,15	–
NGC 6626 ^{B,I}	7.80	-5.58	5.34 ± 0.17	5.5	5.368 ^{+0.099} _{-0.098}	5.6±0.5	3 -8.16	-1.29±0.01	22	12.8 ± 1.0	12
NGC 6637 ^{B,I}	1.72	-10.27	8.80 ± 0.88	8.80	8.900 ^{+0.106} _{-0.104}	8.75±0.12	4 -7.64	-0.59±0.07	4	12.3 ± 0.6	3
NGC 6638 ^I	7.90	-7.15	10.32 ± 1.03	9.40	9.775 ^{+0.347} _{-0.341}	9.6±0.5	3 -7.12	-0.99±0.07	4	12.0	2
NGC 6642 ^{B,I}	9.81	-6.44	8.10 ± 0.81	8.10	8.049 ^{+0.304} _{-0.198}	8.2±0.7	3 -6.66	-1.11±0.14	4	12.7 ± 1.1	1
NGC 6652 ^I	1.53	-11.38	9.51 ± 0.12	10	9.464 ^{+0.137} _{-0.137}	9.34±0.18	4 -6.66	-0.76±0.14	4	12.7 ± 0.7	3
NGC 6717 ^{B,I}	12.88	-10.90	7.14 ± 0.10	7.10	7.524 ^{+0.133} _{-0.131}	7.3±0.5	3 -5.66	-1.26±0.07	4	13.5 ± 0.8	3
NGC 6723 ^I	0.07	-17.30	8.17 ± 0.11	8.70	8.267 ^{+0.100} _{-0.099}	8.09±0.11	4 -7.83	-1.01±0.05	24	12.6 ± 0.6	3

Symbols: ^B identified as a bulge cluster by PV20, ^I identified as in situ by [Belokurov & Kravtsov \(2024\)](#). References to distance by our group: 1 [Barbuy et al. \(1998\)](#); 2 [Ortolani et al. \(1999a\)](#); 3 [Oliveira et al. \(2022\)](#); 4 [Oliveira et al. \(2020\)](#); 5 [Ortolani et al. \(2000\)](#); 6 [Souza et al. \(2023\)](#); 7 [Ortolani et al. \(1997\)](#); 8 [Ortolani et al. \(2007\)](#); 9 [Kerber et al. \(2019\)](#); 10 [Ortolani et al. \(1999b\)](#); 11 [Bica et al. \(1996\)](#); 12 [Barbuy et al. \(1999a\)](#); 13 [Souza et al. \(2021\)](#); 14 [Ortolani et al. \(2019b\)](#); 15 [Ortolani et al. \(1994\)](#); 16 [Barbuy et al. \(1997\)](#); 17 [Ortolani et al. \(1999c\)](#); 18 [Ortolani et al. \(2019a\)](#); 19 [Kerber et al. \(2018\)](#); 20 [Bica et al. \(1994\)](#); 21 [Guarnieri et al. \(1998\)](#); 22 [Rich et al. \(1998\)](#). References to metallicity: 1 [Vázquez et al. \(2018\)](#) from CaT, calibrated to [Dias et al. \(2016\)](#); 2 [Saviane et al. \(2012\)](#); 3 [Simpson et al. \(2017\)](#); 4 [Carretta et al. \(2009\)](#); 5 [Johnson et al. \(2016\)](#); 6 [Souza et al. \(2023\)](#); 7 [Geisler et al. \(2021\)](#); 8 [Origlia & Rich \(2004\)](#); 9 [Barbuy et al. \(2016\)](#); 10 [Crociati et al. \(2023\)](#) from MUSE; 11 [Souza et al. \(2021\)](#); 12 [Massari et al. \(2014\)](#); 13 [Geisler et al. \(2023\)](#) from CaT; 14 [Fernández-Trincado et al. \(2020\)](#); 15 [Ernandes et al. \(2019\)](#) from MUSE; 16 [Barbuy et al. \(2021\)](#) and [Fernández-Trincado et al. \(2019\)](#); 17 [Carretta et al. \(2001\)](#), [Zoccali et al. \(2004\)](#), and [Muñoz et al. \(2018\)](#); 18 [Barbuy et al. \(1999b\)](#), [Meléndez et al. \(2003\)](#), [Alves-Brito et al. \(2006\)](#), [Origlia et al. \(2002\)](#), and [Montecinos et al. \(2021\)](#); 19 [Barbuy et al. \(2018b\)](#) and [González-Díaz et al. \(2023\)](#); 20 [Peñaloza et al. \(2015\)](#); 21 [Husser et al. \(2020\)](#) from MUSE; 22 [Villanova et al. \(2017\)](#); 23 [Crestani et al. \(2019\)](#); 24 [Fernández-Trincado et al. \(2021a\)](#). ** For Terzan 5 and Liller 1, we adopt a mean weighted to the most important multi-population component. References of age: 1 [Cohen et al. \(2021\)](#) with relative ages; 2 [Meisner & Weiss \(2006\)](#); 3 [Oliveira et al. \(2020\)](#); 4 [Souza et al. \(2023\)](#); 5 [Kerber et al. \(2019\)](#); 6 [Ferraro et al. \(2021\)](#); 7 [Souza et al. \(2021\)](#); 8 [Ferraro et al. \(2016\)](#); 9 [Pallanca et al. \(2021\)](#); 10 [Fernández-Trincado et al. \(2020\)](#); 11 [Ortolani et al. \(2019a\)](#); 12 [Kerber et al. \(2018\)](#) with a mean age between Dartmouth and BaSTI models; 13 [Renzini et al. \(2018\)](#); 14 [Bruzual et al. \(1997\)](#); 15 [Saracino et al. \(2016\)](#).

In [Figure 1](#) the location of the bulge clusters is plotted in galactic coordinates, ℓ and b , in degrees. This figure is an update of [figure 3](#) from [Barbuy et al. \(2018a\)](#), including a) the bulge GCs, [Bica et al. \(2016\)](#) b) candidate clusters, and c) newly confirmed clusters. All of the objects from lists b) and c) are new relative to a). UKS 1 is now included as a previously known cluster: it was not included as such in [Bica et al. \(2016\)](#) for the reason that its distance was a limiting case. It still is, but it is a typical bulge cluster in terms of CMD, which justifies its inclusion in the list; its true distance remains an open question.

There are two cases of clusters that had previously been identified at the time of the [Bica et al. \(2016\)](#) review but that had essentially no data, and that have since been observed and characterized in recent surveys, as is shown in [Table 1](#). These clusters

are VVV-CL002 and Kronberger 49, and they are plotted in the figures as new clusters. Therefore, we consider hereafter 42 well-known clusters, comprising those from [Bica et al. \(2016\)](#), except for VVV-CL002 and Kronberger 49, which we took out from [Table 3](#), in addition to UKS 1.

4. Parameters of the new sample

4.1. Metallicity and mass

The sample clusters have lower masses than the well-known GCs, as is indicated by their integrated absolute magnitudes, with most of them with M_V fainter than -7.0 mag. This is clearly seen in [Figure 2](#), where only clusters that have an M_V value

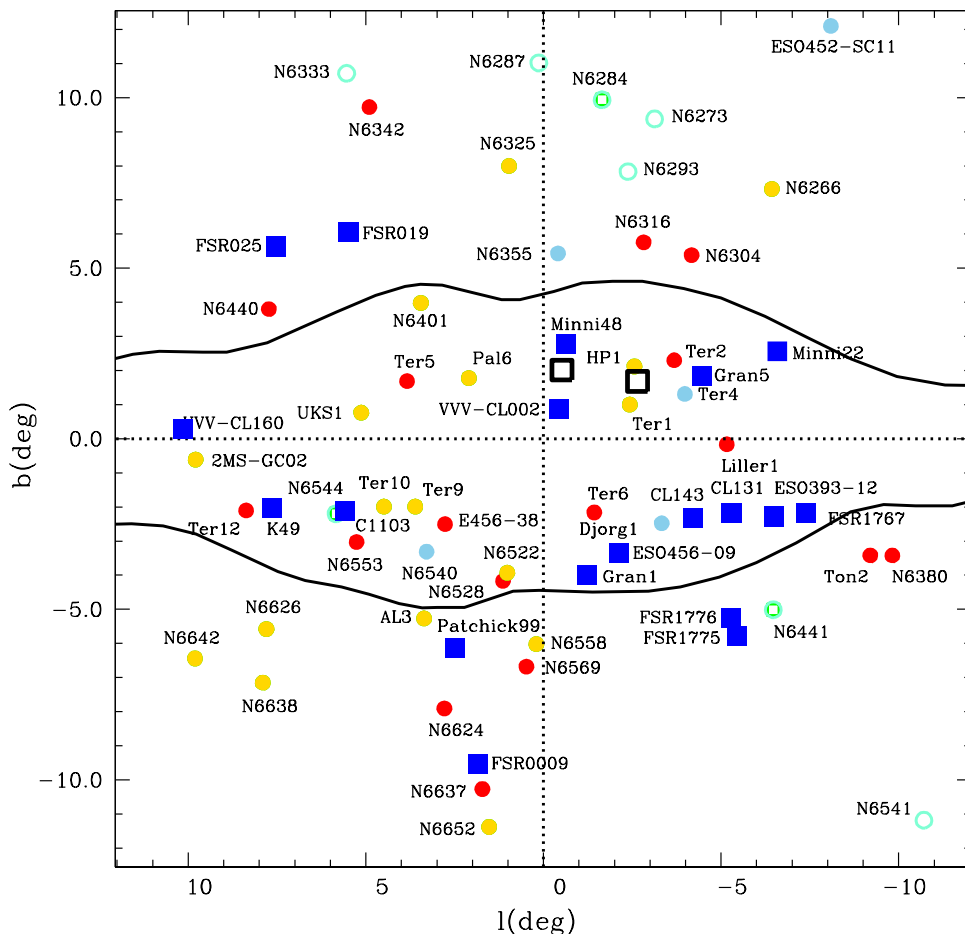


Fig. 1. Location in Galactic coordinates of bulge clusters, including a) projected bulge globular clusters of cf. Bica et al. (2016), represented by filled circles, with $[\text{Fe}/\text{H}] > -0.8$ (red); $-1.3 < [\text{Fe}/\text{H}] < -0.8$ (gold); $[\text{Fe}/\text{H}] < -1.3$ (blue); halo clusters: aquamarine open circles; cluster farther from the Galactic center than $R_c > 4.5$ kpc: green open squares; b) candidate clusters (open black squares); c) newly confirmed clusters located in the region (blue filled squares). The Galactic center is illustrated by the blue filled circle. Contours correspond to COBE/DIRBE outline of the bulge from Weiland et al. (1994), and adapted from Jönsson et al. (2017).

available are included. This figure shows that the new clusters all have low masses relative to the other two samples. It is therefore unlikely that massive clusters are still missing, but there could still be massive clusters with low density that remain undetected. Other low mass clusters probably also remain undetected due to crowding and high extinction. It can be seen in the right panel of Figure 2 that the low-luminosity tail of the globular cluster luminosity function (GCLF) is non-Gaussian, given an extended tail of low-mass clusters (see also the discussion on this matter by Jordán et al. 2007).

Figure 3 shows the metallicity distribution of bulge clusters, including the well-known bulge clusters reported in Table 3, together with the new sample clusters listed in Table 1, excluding the halo, halo intruder, and disk clusters, clusters that have $[\text{Fe}/\text{H}] \lesssim -1.5$ dex (in order to be compatible with the selection criteria of bulge clusters defined in Bica et al. 2016), and clusters that have distances out of the range of $4 \lesssim d_{\odot} \lesssim 11$ kpc.

The left panel shows the histogram of metallicity and the right panel kernel density estimations. From the right panel of Fig. 3 the combined bulge sample (Tables 1 and 3) show peaks at $[\text{Fe}/\text{H}] \sim -1.08 \pm 0.35$ and -0.51 ± 0.25 dex. The more metal-poor peak is in agreement with that of Bica et al. (2016), whereas the more metal-rich peak is shifted by ~ 0.1 dex compared to Bica et al. (2016) due to the large number of new clusters with $[\text{Fe}/\text{H}] \sim -0.6$ dex. The new clusters alone have peaks at $[\text{Fe}/\text{H}] \sim -0.55$ dex, coincident with the full sample, and at a lower metallicity of $[\text{Fe}/\text{H}] \sim -1.2$ dex, but with low statistics.

The seven new halo clusters are all more metal-poor than $[\text{Fe}/\text{H}] < -1.3$ dex, except for VVV-CL003. VVV-CL001 is more metal-poor than any halo cluster, with $[\text{Fe}/\text{H}] \sim -2.45$ dex (Fernández-Trincado et al. 2021b), and it has been suggested, owing to its orbit, that it belongs to a massive dwarf galaxy such as Gaia-Enceladus-Sausage (GES; Belokurov et al. 2018; Helmi et al. 2018) or Sequoia (Seq.; Massari et al. 2019) that merged with the Galaxy at an early time. Another cluster with such low metallicity in the bulge is ESO 280-SC06 (Ortolani et al. 2000), which was recently studied spectroscopically, revealing a metallicity of $[\text{Fe}/\text{H}] = -2.48$ dex by Simpson (2018), and reported to be associated with the Gaia-Enceladus-Sausage (Massari et al. 2019) dwarf galaxy.

The bulge field surveys GIBS (Zoccali et al. 2017) and ARGOS (Ness et al. 2013) show peaks at $[\text{Fe}/\text{H}] \sim +0.3$, -0.4 dex and $[\text{Fe}/\text{H}] \sim +0.15$, -0.25 , and -0.7 dex, respectively. The combined sample of bulge clusters shows compatibility between bulge clusters and the field at $[\text{Fe}/\text{H}] \sim -0.5$ dex from (Zoccali et al. 2017), and $[\text{Fe}/\text{H}] \sim -0.7$ dex from (Ness et al. 2013). The more metal-poor peak at $[\text{Fe}/\text{H}] \sim -1.1$ dex already pointed out in Bica et al. (2016) is confirmed here.

4.2. Ages

Regarding ages, only 28 of the new sample clusters have values of age and metallicity reported in the literature.

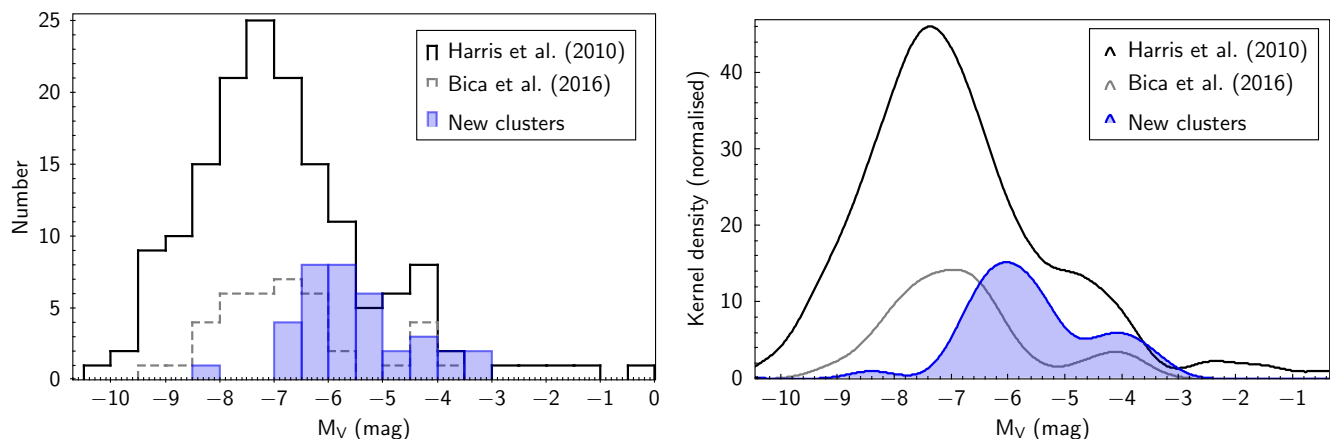


Fig. 2. Absolute magnitude, M_V , of the new cluster sample compared to the literature. (*Left panel:*) Histogram of the 36 of the 41 new clusters from Table 1 with available M_V (solid blue histogram), compared to H10 (156 clusters, solid black histogram) and bulge clusters Bica et al. (2016, 42 clusters) plus UKS 1 (dashed gray histogram). (*Right panel:*) Kernel density estimation of the three distributions, with a Gaussian kernel and normalized y axis. A low-luminosity tail is seen in the three samples between $M_V \sim -5$ and -4 mag.

The ages were obtained from the visual fitting of isochrones. The CMDs are not deep, with those from VVV data reaching $K_S \sim 17 - 18$ mag, in the best cases; those from WISE data are shallow, with $K_S \sim 14 - 15$ mag. Garro et al. (2022b) give an age uncertainty of ± 2 Gyr, while Fernández-Trincado et al. (2022) give ± 3 Gyr. We can adopt a general uncertainty of $\pm 2 - 3$ Gyr. In order to have a comparison sample of clusters formed in situ, and another sample formed ex situ, we adopt the selection by Forbes & Bridges (2010) and Forbes (2020), with data updated in Kruijssen et al. (2019), and Limberg et al. (2022). These samples were intended to verify an AMR of the new clusters from Table 1.

Figure 4 compares the complete sample of well-known bulge clusters, plus the new sample, to clusters from the dwarf galaxies Sagittarius and Canis Majoris listed in Forbes & Bridges (2010), and from Gaia-Enceladus-Sausage listed in Limberg et al. (2022).

Figure 4 gives a metallicity versus age for the new clusters that have these values available, excluding seven clusters that have no measurement of proper motion and/or radial velocity. They are compared with the Bica et al. (2016) sample, and with the Sagittarius and Canis Majoris clusters identified in Forbes & Bridges (2010), and updates from Kruijssen et al. (2019), plus Gaia-Enceladus-Sausage clusters and the age-metallicity curve from Limberg et al. (2022). This figure shows that all known in situ bulge clusters are older than > 11.5 Gyr, and do not follow an AMR, as is shown by the solid line at 12.5 Gyr. This is the case of a fraction of the new clusters, whereas the other clusters follow the AMR of the ex situ clusters from the dwarf galaxies. Although the age-metallicity curves of different dwarf galaxies are somewhat different, as can be seen for example in Figure 9 of Callingham et al. (2022), they are sufficiently close for us to plot that relation from Gaia-Enceladus-Sausage.

For a deeper study, better derivations of ages with deeper photometric data are needed. We also note that for AMRs it is important to have relative ages, as well as homogeneous derivations of ages, as is discussed by, for example, Dotter et al. (2011), Vandenberg et al. (2013), and Leaman et al. (2013). We recognize that there are likely systematic differences between the different studies that are at least as large as the assigned random errors. However, a homogenization of ages cannot be found in the literature for either the well-known bulge clusters or the newly identified clusters.

Finally, radial velocity measurements are required to study the cluster orbits. Therefore, no firm conclusion can be drawn yet for the clusters with ages estimated to be lower than 10 Gyr, but in principle they are compatible with an ex situ origin.

4.3. Distances

Figure 5 shows the histogram and distribution of distances to the Sun for the new bulge clusters (Table 1) compared with the compiled distances from Bica et al. (2016, Table 3) and with the full cluster sample. The samples are the same as in Figure 3 except for the cluster Glimpse02, which has no available distance in the literature.

The histogram of new clusters shows two peaks at 7.2 and 8.5 kpc, but the kernel density estimation shows them as a smooth distribution centered around 8.0 kpc. This configuration of the histogram remains for different distance bins. The full cluster sample preserves the distance distribution from Bica et al. (2016), with a peak around 8.0 – 8.1 kpc and a tail pointing to smaller distances. The peak is compatible, within 0.2 kpc, with the Galactic Black Hole distance of $d_{GC\text{Center}} = 8.178 \pm 0.013_{\text{stat.}} \pm 0.022_{\text{sys.}}$ kpc (GRAVITY Collaboration et al. 2019). More recently, Arakelyan et al. (2018) have found 8.2 kpc using GCs and dwarf galaxies, but although this might appear obvious now, it was not the case with the data available at the time of our estimation of $d_{GC\text{Center}} = 7.5$ kpc Bica et al. (2006). Bland-Hawthorn & Gerhard (2016) and Griv et al. (2023) provide a historical review of this value.

There is another issue regarding distances, which is the selective-to-total absorption R_V value. While the subject is debated, the recent papers by Nataf et al. (2013), Nataf (2016), and Nataf et al. (2021) lean toward a low reddening slope with $R_V = 2.5$. Pottasch & Bernard-Salas (2013), on the other hand, oppose this conclusion (see Stenborg 2016), based on the analysis of spectra of planetary nebulae in the Galactic bulge (at $b \sim 3 - 6^\circ$). These authors conclude with a strong statement: “The suggestion that R_V is different in the Galactic bulge is incorrect. The reasons for this are discussed.” A reddening problem is also suggested by Vasiliev & Baumgardt (2021), comparing Gaia Early DR3 parallaxes with optical distances of bulge clusters. The inverted parallaxes give longer distances than the optical ones.

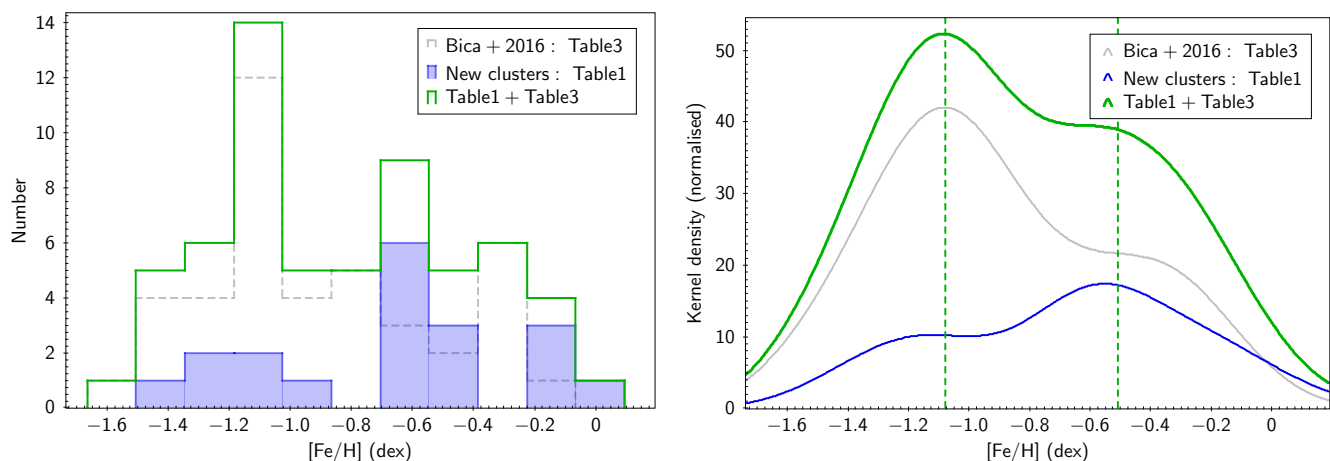


Fig. 3. Metallicities of full sample of bulge clusters. (*Left panel:*) Histogram of metallicity including the 42 well-known bulge clusters from [Bica et al. \(2016\)](#) and the new sample clusters, excluding clusters classified as belonging to the halo and disk, those that have $[\text{Fe}/\text{H}] < -1.5$ dex, and clusters that have distances out of the range of $4 < d_{\odot} < 11$ kpc. A histogram combining both samples is also shown in green. (*Right panel:*) Kernel density estimation, showing the distribution peaks independently of the bin size: [Bica et al. \(2016\)](#) with peaks in -1.05 and -0.40 dex, the new cluster sample with peaks in -1.20 and -0.55 dex, and the combined sample with a higher peak consistent with [Bica et al. \(2016\)](#) but with a smaller peak shifted to a more metal-poor value (dashed lines: -1.08 ± 0.35 and -0.51 ± 0.25 dex).

Some questions remain, however, such as why we should have such an anomalous reddening law. There is no evidence around the Sun of a reddening law with $R_V < 3$. We may eventually have much higher values.

Another question is whether we have an additional problem of a limiting distance, or a peculiar cloud, between us and the bulge, and in that case where it is. [Nataf et al. \(2021\)](#) discusses a peculiar “great dark lane” when citing [Minniti et al. \(2014\)](#), but there is no theoretical support for this, and it would need very large dust grains. The point is not negligible, because it can also introduce a bias in the age measurements with the isochrones, inducing a trend of age versus Galactocentric distance.

The comparison of the *Gaia* Early DR3 distances by [Baumgardt & Vasiliev \(2021\)](#), hereafter BV21) with those given in the literature for the new clusters, however, does not help because of the uncertainties in the parallaxes.

5. Conclusions

We compiled a sample of 39 new GCs and two candidates, mostly in the Galactic bulge, which have been identified since the [Harris \(1996, 2010 edition\)](#) catalog and [Bica et al. \(2016\)](#). The number of confirmed bulge GCs in the Galaxy has considerably increased, with the difference being that the new clusters have very low masses. The new full sample of bulge clusters shows a metallicity distribution with peaks at $[\text{Fe}/\text{H}] = -1.08 \pm 0.35$ and -0.51 ± 0.25 dex.

The age-metallicity plot shows two different aspects: all well-known bulge clusters are older than 11.5 Gyr, and 13 of the new clusters are in this category; that is, they are all old and no AMR is seen, as has been shown by studies in the literature, such as those by [Forbes & Bridges \(2010\)](#), [Forbes \(2020\)](#), [Krujissen et al. \(2020\)](#), and [Callingham et al. \(2022\)](#).

For the 11 clusters younger than 11.5 Gyr, the AMR appears to be compatible with that of the ex situ dwarf galaxies Sagittarius, Canis Majoris, and Gaia-Enceladus-Sausage.

Finally, we conclude that it is likely that very few, if any, other massive GCs in the Galactic bulge are still to be found, although we cannot exclude that massive clusters with low densities remain undetected. Given the dense environment, it is ex-

pected that some of the lowest mass clusters could also be dispersing, and thus be missed in the dense bulge field.

A next step in the study of these clusters should be spectroscopic analyses, in particular to derive their radial velocities. This will allow us to derive their orbits and to better understand their origin.

Acknowledgements. We are grateful to the referee for very helpful suggestions, and to Stefano O. Souza for helpful comments. EB and BB acknowledge partial financial support from CAPES - Finance code 001, CNPq and FAPESP. SO acknowledges support from PRIN MIUR2022 Progetto “CHRONOS” (PI: S. Casisi) financed by the European Union - Next Generation EU, the support of the University of Padova, DOR Piotta 2022, Italy. RAPO acknowledges the FAPESP PhD fellowship 2018/22181-0.

References

- Alves-Brito, A., Barbuy, B., Zoccali, M., et al. 2006, *A&A*, 460, 269
 Arakelyan, N. R., Pilipenko, S. V., & Libeskind, N. I. 2018, *MNRAS*, 481, 918
 Barbá, R. H., Minniti, D., Geisler, D., et al. 2019, *ApJ*, 870, L24
 Barbuy, B., Cantelli, E., Muniz, L., et al. 2021, *A&A*, 654, A29
 Barbuy, B., Cantelli, E., Vemado, A., et al. 2016, *A&A*, 591, A53
 Barbuy, B., Chiappini, C., & Gerhard, O. 2018a, *ARA&A*, 56, 223
 Barbuy, B., Muniz, L., Ortolani, S., et al. 2018b, *A&A*, 619, A178
 Barbuy, B., Ortolani, S., & Bica, E. 1997, *A&AS*, 122, 483
 Barbuy, B., Ortolani, S., & Bica, E. 1998, *A&AS*, 132, 333
 Barbuy, B., Ortolani, S., Bica, E., & Desidera, S. 1999a, *A&A*, 348, 783
 Barbuy, B., Renzini, A., Ortolani, S., Bica, E., & Guarnieri, M. D. 1999b, *A&A*, 341, 539
 Barbuy, B., Zoccali, M., Ortolani, S., et al. 2009, *A&A*, 507, 405
 Baumgardt, H. & Vasiliev, E. 2021, *MNRAS*, 505, 5957
 Belokurov, V., Erkal, D., Evans, N. W., Koposov, S. E., & Deason, A. J. 2018, *MNRAS*, 478, 611
 Belokurov, V. & Kravtsov, A. 2024, *MNRAS*, 528, 3198
 Bica, E., Bonatto, C., Barbuy, B., & Ortolani, S. 2006, *A&A*, 450, 105
 Bica, E., Ortolani, S., & Barbuy, B. 1994, *A&A*, 283, 67
 Bica, E., Ortolani, S., & Barbuy, B. 1996, *A&AS*, 120, 153
 Bica, E., Ortolani, S., & Barbuy, B. 2016, *PASA*, 33, e028
 Bica, E., Pavani, D. B., Bonatto, C. J., & Lima, E. F. 2019, *AJ*, 157, 12
 Bland-Hawthorn, J. & Gerhard, O. 2016, *ARA&A*, 54, 529
 Borissova, J., Ivanov, V. D., Lucas, P. W., et al. 2018, *MNRAS*, 481, 3902
 Bressan, A., Fagotto, F., Bertelli, G., & Chiosi, C. 1993, *A&AS*, 100, 647
 Bruzual, G., Barbuy, B., Ortolani, S., et al. 1997, *AJ*, 114, 1531
 Butler, E., Kunder, A., Prudil, Z., et al. 2024, *ApJ*, 963, L33
 Callingham, T. M., Cautun, M., Deason, A. J., et al. 2022, *MNRAS*, 513, 4107
 Camargo, D. 2018, *ApJ*, 860, L27
 Camargo, D. & Minniti, D. 2019, *MNRAS*, 484, L90

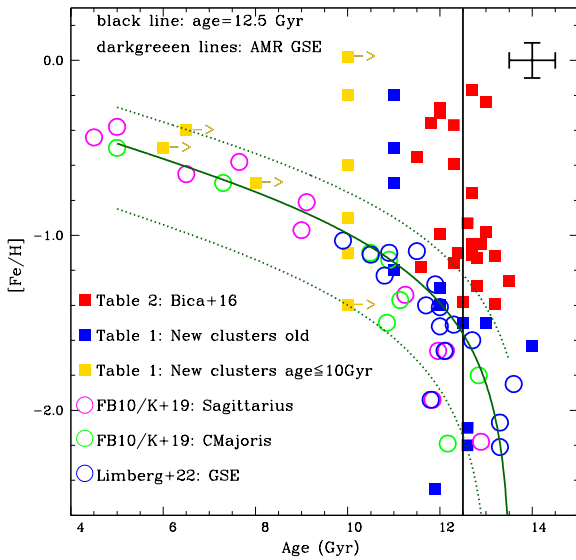


Fig. 4. Metallicity vs. age for the new clusters that have these values available, compared with the Bica et al. (2016) sample, and with the Sagittarius and Canis Majoris clusters identified in Forbes & Bridges (2010) labeled as FB10, with updates from Kruijssen et al. (2019) labeled as K+19, and Gaia-Enceladus-Sausage with clusters identified in Limberg et al. (2022). Bulge clusters from Table 3 are represented by filled red squares; old clusters from Table 1 by filled blue squares; clusters from Table 1 younger than 10 Gyr by filled gold squares; clusters from Sagittarius by open magenta circles; clusters from Canis Majoris by open green circles; clusters from GSE by open blue circles; ages of 12.5 ± 0.3 Gyr by black lines; and the model and uncertainties from Forbes & Bridges (2010) by green lines. The old bulge clusters are all old and show no AMR, as is indicated by the straight black line with an age of 12.0 Gyr. Dark green curves represent the best fit of the AMR to the GSE sample from Limberg et al. (2022), and $\pm 3\sigma$ curves. The lower age limits for five of the new clusters are represented by arrows. The error bar in the upper right corner indicates the typical errors of 0.2 dex in $[\text{Fe}/\text{H}]$ and 1.0 Gyr in age.

Carretta, E., Bragaglia, A., Gratton, R., D’Orazi, V., & Lucatello, S. 2009, *A&A*, 508, 695
 Carretta, E., Cohen, J. G., Gratton, R. G., & Behr, B. B. 2001, *AJ*, 122, 1469
 Cohen, R. E., Bellini, A., Casagrande, L., et al. 2021, *AJ*, 162, 228
 Crestani, J., Alves-Brito, A., Bono, G., Puls, A. A., & Alonso-García, J. 2019, *MNRAS*, 487, 5463
 Crociati, C., Valenti, E., Ferraro, F. R., et al. 2023, *ApJ*, 951, 17
 Dias, B., Barbuy, B., Saviane, I., et al. 2016, *A&A*, 590, A9
 Dias, B., Palma, T., Minniti, D., et al. 2022, *A&A*, 657, A67
 Dotter, A., Chaboyer, B., Jevremović, D., et al. 2008, *ApJS*, 178, 89
 Dotter, A., Sarajedini, A., & Anderson, J. 2011, *ApJ*, 738, 74
 Fernandes, H., Dias, B., Barbuy, B., et al. 2019, *A&A*, 632, A103
 Fernández-Trincado, J. G., Beers, T. C., Minniti, D., et al. 2021a, *A&A*, 647, A64
 Fernández-Trincado, J. G., Minniti, D., Beers, T. C., et al. 2020, *A&A*, 643, A145
 Fernández-Trincado, J. G., Minniti, D., Garro, E. R., & Villanova, S. 2022, *A&A*, 657, A84
 Fernández-Trincado, J. G., Minniti, D., Souza, S. O., et al. 2021b, *ApJ*, 908, L42
 Fernández-Trincado, J. G., Zamora, O., Souto, D., et al. 2019, *A&A*, 627, A178
 Ferraro, F. R., Massari, D., Dalessandro, E., et al. 2016, *ApJ*, 828, 75
 Ferraro, F. R., Pallanca, C., Lanzoni, B., et al. 2021, *Nature Astronomy*, 5, 311
 Forbes, D. A. 2020, *MNRAS*, 493, 847
 Forbes, D. A. & Bridges, T. 2010, *MNRAS*, 404, 1203
 Gaia Collaboration, Vallenari, A., Brown, A. G. A., et al. 2023, *A&A*, 674, A1
 Garro, E. R., Fernández-Trincado, J. G., Minniti, D., et al. 2023, *A&A*, 669, A136
 Garro, E. R., Minniti, D., Alessi, B., et al. 2022a, *A&A*, 659, A155
 Garro, E. R., Minniti, D., Gómez, M., et al. 2020, *A&A*, 642, L19
 Garro, E. R., Minniti, D., Gómez, M., et al. 2021, *A&A*, 649, A86
 Garro, E. R., Minniti, D., Gómez, M., et al. 2022b, *A&A*, 658, A120

Garro, E. R., Minniti, D., Gómez, M., et al. 2022c, *A&A*, 662, A95
 Geisler, D., Parisi, M. C., Dias, B., et al. 2023, *A&A*, 669, A115
 Geisler, D., Villanova, S., O’Connell, J. E., et al. 2021, *A&A*, 652, A157
 González-Díaz, D., Fernández-Trincado, J. G., Villanova, S., et al. 2023, *MNRAS*, 526, 6274
 Gran, F., Kordopatis, G., Zoccali, M., et al. 2024, *A&A*, 683, A167
 Gran, F., Zoccali, M., Contreras Ramos, R., et al. 2019, *A&A*, 628, A45
 Gran, F., Zoccali, M., Saviane, I., et al. 2022, *MNRAS*, 509, 4962
 GRAVITY Collaboration, Abuter, R., Amorim, A., et al. 2019, *A&A*, 625, L10
 Griv, E., Jiang, I.-G., Majaess, D., & Minniti, D. 2023, *Astrophys. Space Sci.*, 368
 Guarnieri, M. D., Ortolani, S., Montegriffo, P., et al. 1998, *A&A*, 331, 70
 Harris, W. E. 1996, *AJ*, 112, 1487
 Helmi, A., Babusiaux, C., Koppelman, H. H., et al. 2018, *Nature*, 563, 85
 Horta, D., Schiavon, R. P., Mackereth, J. T., et al. 2023, *MNRAS*, 520, 5671
 Husser, T.-O., Latour, M., Brinchmann, J., et al. 2020, *A&A*, 635, A114
 Ivanov, V. D., Kurtev, R., & Borissova, J. 2005, *A&A*, 442, 195
 Johnson, C. I., Caldwell, N., Rich, R. M., Pilachowski, C. A., & Hsyu, T. 2016, *AJ*, 152, 21
 Jönsson, H., Ryde, N., Schultheis, M., & Zoccali, M. 2017, *A&A*, 598, A101
 Jordán, A., McLaughlin, D. E., Côté, P., et al. 2017, *ApJS*, 171, 101
 Kerber, L. O., Libralato, M., Souza, S. O., et al. 2019, *MNRAS*, 484, 5530
 Kerber, L. O., Nardiello, D., Ortolani, S., et al. 2018, *ApJ*, 853, 15
 Kruijssen, J. M. D., Pfeffer, J. L., Chevance, M., et al. 2020, *MNRAS*, 498, 2472
 Kruijssen, J. M. D., Pfeffer, J. L., Reina-Campos, M., Crain, R. A., & Bastian, N. 2019, *MNRAS*, 486, 3180
 Kurtev, R., Ivanov, V. D., Borissova, J., & Ortolani, S. 2008, *A&A*, 489, 583
 Leaman, R., VandenBerg, D. A., & Mendel, J. T. 2013, *MNRAS*, 436, 122
 Limberg, G., Souza, S. O., Pérez-Villegas, A., et al. 2022, *ApJ*, 935, 109
 Marín-Franch, A., Aparicio, A., Piotto, G., et al. 2009, *ApJ*, 694, 1498
 Massari, D., Koppelman, H. H., & Helmi, A. 2019, *A&A*, 630, L4
 Massari, D., Mucciarelli, A., Ferraro, F. R., et al. 2014, *ApJ*, 795, 22
 Meissner, F. & Weiss, A. 2006, *A&A*, 456, 1085
 Meléndez, J., Barbuy, B., Bica, E., et al. 2003, *A&A*, 411, 417
 Minniti, D., Fernández-Trincado, J. G., Gómez, M., et al. 2021a, *A&A*, 650, L11
 Minniti, D., Fernández-Trincado, J. G., Smith, L. C., et al. 2021b, *A&A*, 648, A86
 Minniti, D., Hempel, M., Toledo, I., et al. 2011, *A&A*, 527, A81
 Minniti, D., Lucas, P. W., Emerson, J. P., et al. 2010, *New A*, 15, 433
 Minniti, D., Matsunaga, N., Fernández-Trincado, J. G., et al. 2024, *A&A*, 683, A150
 Minniti, D., Palma, T., Camargo, D., et al. 2021c, *A&A*, 652, A129
 Minniti, D., Saito, R. K., Gonzalez, O. A., et al. 2014, *A&A*, 571, A91
 Minniti, D., Schlafly, E. F., Palma, T., et al. 2018, *ApJ*, 866, 12
 Moni Bidin, C., Mauro, F., Geisler, D., et al. 2011, *A&A*, 535, A33
 Montecinos, C., Villanova, S., Muñoz, C., & Cortés, C. C. 2021, *MNRAS*, 503, 4336
 Muñoz, C., Geisler, D., Villanova, S., et al. 2018, *A&A*, 620, A96
 Myeong, G. C., Vasiliev, E., Iorio, G., Evans, N. W., & Belokurov, V. 2019, *MNRAS*, 488, 1235
 Nataf, D. M. 2016, *PASA*, 33, e024
 Nataf, D. M., Cassisi, S., Casagrande, L., Yuan, W., & Riess, A. G. 2021, *ApJ*, 910, 121
 Nataf, D. M., Gould, A., Fouqué, P., et al. 2013, *ApJ*, 769, 88
 Ness, M., Freeman, K., Athanassoula, E., et al. 2013, *MNRAS*, 430, 836
 Obasi, C., Gómez, M., Minniti, D., & Alonso-García, J. 2021, *A&A*, 654, A39
 Oliveira, R. A. P., Ortolani, S., Barbuy, B., et al. 2022, *A&A*, 657, A123
 Oliveira, R. A. P., Souza, S. O., Kerber, L. O., et al. 2020, *ApJ*, 891, 37
 Origlia, L. & Rich, R. M. 2004, *AJ*, 127, 3422
 Origlia, L., Rich, R. M., & Castro, S. 2002, *AJ*, 123, 1559
 Ortolani, S., Barbuy, B., & Bica, E. 1994, *A&AS*, 108, 653
 Ortolani, S., Barbuy, B., & Bica, E. 1999a, *A&AS*, 136, 237
 Ortolani, S., Barbuy, B., Bica, E., et al. 1999b, *A&A*, 350, 840
 Ortolani, S., Barbuy, B., Bica, E., Zoccali, M., & Renzini, A. 2007, *A&A*, 470, 1043
 Ortolani, S., Bica, E., & Barbuy, B. 1997, *A&A*, 326, 614
 Ortolani, S., Bica, E., & Barbuy, B. 1999c, *A&AS*, 138, 267
 Ortolani, S., Bica, E., & Barbuy, B. 2000, *A&A*, 361, L57
 Ortolani, S., Bonatto, C., Bica, E., Barbuy, B., & Saito, R. K. 2012, *AJ*, 144, 147
 Ortolani, S., Held, E. V., Nardiello, D., et al. 2019a, *A&A*, 627, A145
 Ortolani, S., Nardiello, D., Pérez-Villegas, A., Bica, E., & Barbuy, B. 2019b, *A&A*, 622, A94
 Pallanca, C., Lanzoni, B., Ferraro, F. R., et al. 2021, *ApJ*, 913, 137
 Peñaloza, F., Pessev, P., Vázquez, S., et al. 2015, *PASP*, 127, 329
 Pérez-Villegas, A., Barbuy, B., Kerber, L. O., et al. 2020, *MNRAS*, 491, 3251
 Pietrinferni, A., Cassisi, S., Salaris, M., & Castelli, F. 2006, *ApJ*, 642, 797
 Pottasch, S. R. & Bernard-Salas, J. 2013, *A&A*, 550, A35
 Queiroz, A. B. A., Anders, F., Chiappini, C., et al. 2020, *A&A*, 638, A76
 Queiroz, A. B. A., Chiappini, C., Perez-Villegas, A., et al. 2021, *A&A*, 656, A156

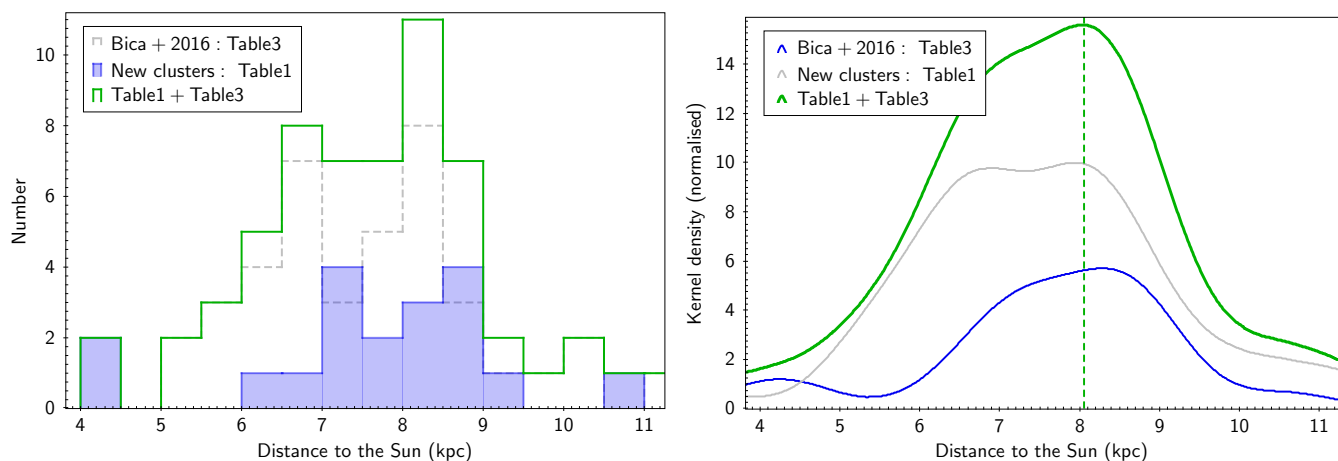


Fig. 5. Distribution of distances of the same cluster sample as in Figure 3. Despite having the same smoothing, the kernel density estimations are noisier than the metallicity ones, but show that the Bica et al. (2016) and the full samples share a peak around 8.0 – 8.1 kpc, as was expected.

- Renzini, A., Gennaro, M., Zoccali, M., et al. 2018, *ApJ*, 863, 16
 Rich, R. M., Ortolani, S., Bica, E., & Barbuy, B. 1998, *AJ*, 116, 1295
 Ryu, J. & Lee, M. G. 2018, *ApJ*, 863, L38
 Saracino, S., Dalessandro, E., Ferraro, F. R., et al. 2016, *ApJ*, 832, 48
 Saviane, I., Da Costa, G. S., Held, E. V., et al. 2012, *A&A*, 540, A27
 Simpson, J. D. 2018, *MNRAS*, 477, 4565
 Simpson, J. D., De Silva, G., Martell, S. L., Navin, C. A., & Zucker, D. B. 2017, *MNRAS*, 472, 2856
 Souza, S. O., Ernandes, H., Valentini, M., et al. 2023, *A&A*, 671, A45
 Souza, S. O., Kerber, L. O., Barbuy, B., et al. 2020, *ApJ*, 890, 38
 Souza, S. O., Valentini, M., Barbuy, B., et al. 2021, *A&A*, 656, A78
 Stenborg, T. N. 2016, PhD thesis, Macquarie University, Department of Physics and Astronomy
 VandenBerg, D. A., Bergbusch, P. A., Ferguson, J. W., & Edvardsson, B. 2014, *ApJ*, 794, 72
 VandenBerg, D. A., Brogaard, K., Leaman, R., & Casagrande, L. 2013, *ApJ*, 775, 134
 Vasiliev, E. & Baumgardt, H. 2021, *MNRAS*, 505, 5978
 Vázquez, S., Saviane, I., Held, E. V., et al. 2018, *A&A*, 619, A13
 Villanova, S., Monaco, L., Geisler, D., et al. 2019, *ApJ*, 882, 174
 Villanova, S., Moni Bidin, C., Mauro, F., Muñoz, C., & Monaco, L. 2017, *MNRAS*, 464, 2730
 Weiland, J. L., Arendt, R. G., Berriman, G. B., et al. 1994, *ApJ*, 425, L81
 Wright, E. L., Eisenhardt, P. R. M., Mainzer, A. K., et al. 2010, *AJ*, 140, 1868
 Zoccali, M., Barbuy, B., Hill, V., et al. 2004, *A&A*, 423, 507
 Zoccali, M., Vázquez, S., Gonzalez, O. A., et al. 2017, *A&A*, 599, A12